Towards quantitative atmospheric water vapor profiling with differential absorption lidar

Alex Dinovitser,[1,2] **Lachlan J. Gunn,**[2] **and Derek Abbott** [2]

[1]*School of Chemistry and Physics, University of Adelaide, SA 5005, Australia*
[2]*School of Electrical & Electronic Engineering, University of Adelaide, SA 5005, Australia*
alex.dinovitser@adelaide.edu.au

Abstract: Differential Absorption Lidar (DIAL) is a powerful laser-based technique for trace gas profiling of the atmosphere. However, this technique is still under active development requiring precise and accurate wavelength stabilization, as well as accurate spectroscopic parameters of the specific resonance line and the effective absorption cross-section of the system. In this paper we describe a novel master laser system that extends our previous work for robust stabilization to virtually any number of multiple side-line laser wavelengths for the future probing to greater altitudes. In this paper, we also highlight the significance of laser spectral purity on DIAL accuracy, and illustrate a simple re-arrangement of a system for measuring effective absorption cross-section. We present a calibration technique where the laser light is guided to an absorption cell with 33 m path length, and a quantitative number density measurement is then used to obtain the effective absorption cross-section. The same absorption cell is then used for on-line laser stabilization, while microwave beat-frequencies are used to stabilize any number of off-line lasers. We present preliminary results using $\sim$300 nJ, 1 μs pulses at 3 kHz, with the seed laser operating as a nanojoule transmitter at 822.922 nm, and a receiver consisting of a photomultiplier tube (PMT) coupled to a 356 mm mirror.

OCIS codes: (120.0120) Instrumentation, measurement, and metrology; (280.0280) Remote sensing and sensors; (300.6260) Spectroscopy, diode lasers; (280.1910) DIAL, differential absorption lidar; (140.3425) Laser stabilization; (120.0280) Remote sensing and sensors; (010.1280) Atmospheric composition; (010.3920) Meteorology; (010.7340) Water.

References and links

1. J. R. Chen, K. Numata, S. T. Wu, "Error reduction methods for integrated-path differential-absorption lidar measurements," Opt. Express **20** 15589–15609 (2012).
2. M. A. Krainak, J. B. Abshire, J. Camp, J. R. Chen, B. Coyle, S. X. Li, K. Numata, H. Riris, M. A. Stephen, P. Stysley, G. Yang and A. W. Yu, "Laser transceivers for future NASA missions," Proc. SPIE Laser Technology for Defense and Security VIII, **8381** 83810Y (2012).
3. T. F. Refaat, S. Ismail, A. R. Nehrir, J. W. Hair, J. H. Crawford, I. Leifer, T. Shuman, "Performance evaluation of a 1.6 μm methane DIAL system from ground, aircraft and UAV platforms," Opt. Express **25** 30415–30432 (2013).
4. R. M. Schotland, "Some observations of the vertical profile of water vapor by means of a ground based optical radar," Proc. Fourth Symposium on Remote Sensing of the Environment, Ann Arbor, Michigan, 12–24 April, Environmental Research Institute of Michigan, 273–283 (1966).
5. V. Wulfmeyer and J. Boesenberg, "Ground-based differential absorption lidar for water-vapor profiling: assessment of accuracy, resolution, and meteorological applications," Appl. Opt. **37**, 3825–3844 (1998).

#243917 Received 30 Jun 2015; accepted 13 Aug 2015; published 21 Aug 2015

6. A. Sennaroglu, *Solid-State Lasers and Applications* (CRC press, 2006), Chap. 12
7. L. S. Rothman, I. E. Gordon, A. Barbe, D. C. Benner, P. F. Bernath, M. Birk, V. Boudon, L. R. Brown, A. Campargue, J. P. Champion, K. V. Chance, L. H. Coudert, V. Dana, V. M. Devi, S. Fally, J. M. Flaud, R. R. Gamache, A. Goldman, D. Jacquemart, I. Kleiner, N. Lacome, W. J. Lafferty, J. Y. Mandin, S. T. Massie, S. N. Mikhailenko, C. E. Miller, N. Moazzen-Ahmadi, O. V. Naumenko, A. V. Nikitin, J. Orphal, V. I. Perevalov, A. Perrin, A. Predoi-Cross, C. P. Rinsland, M. Rotger, M. Simeckova, M. A. H. Smith, K. Sung, S. A. Tashkun, J. Tennyson, R. A. Toth, A. C. Vandaele and J. V. Auwera, "The HITRAN 2008 molecular spectroscopic database," J. Quant. Spectrosc. Radiat. Transf. **110** 533–572 (2009).
8. P. L. Ponsardin and E. V. Browell, "Measurements of $H_2^{16}O$ linestrengths and air-induced broadenings and shifts in the 815 nm spectral region," J. Mol. Spectrosc. **185,** 58–70 (1997).
9. G. J. Koch, J. Y. Beyon, F. Gibert, B. W. Barnes, S. Ismail, M. Petros, P. J. Petzar, J. Yu, E. A. Modlin, K. J. Davis and U. N. Singh, "Side-line tunable laser transmitter for differential absorption lidar measurements of CO_2: design and application to atmospheric measurements," Appl. Opt. **47** 944–956 (2008).
10. A. S. Moore Jr, K. E. Brown, W. M. Hall, J. C. Barnes, W. C. Edwards, L. B. Petway, A. D. Little, W. S. Luck Jr., Jones, W. J. Irby, C. W. Antill Jr., E. V. Browell and S. Ismail, "Development of the lidar atmospheric sensing experiment (LASE)—An advanced airborne DIAL instrument," in *Advances in Atmospheric Remote Sensing with Lidar* (Springer-Verlag, 1996), pp. 281–288.
11. E. V. Browell, S. Ismail, and W. B. Grant,"Differential absorption lidar (DIAL) measurements from air and space," Appl. Phys. B **67**, 399–410 (1998).
12. E. Grard, D. G. H. Tan, L. Garand, V. Wulfmeyer, G. Ehret, and P. Di Girolamo, "Major advances foreseen in humidity profiling from the water vapor lidar experiment in space (WALES)," Bull. Am. Meteorol. Soc. **85**, 237–251 (2004).
13. G. Wagner, A. Behrendt, V. Wulfmeyer, F. Späth, M. Schiller,"High-power Ti:sapphire laser at 820 nm for scanning ground-based water vapor differential absorption lidar," Appl. Opt. **52** 2454–2469 2013.
14. European Space Agency, J. Callies, R. C. M. Learner, R. Schermaul, N. F. Zobov, D. A. Newnham, J. Ballard and J. Tennyson, "Measurement of H_2O absorption cross-sections," [Internet]. NCAS British Atmospheric Data Centre, 2000–2014.
15. E. E. Whiting, "An empirical approximation to the Voigt profile," Journal of Quantitative Spectroscopy and Radiative Transfer **8,** 1379–1384 (1968).
16. J. J. Olivero and R. L. Longbothum, "Empirical fits to the Voigt line width: A brief review," J. Quant. Spectrosc. Radiat. Transf. **17,** 233–236 (1977).
17. J. L. Machol, T. Ayers, K. T. Schwenz, K. W. Koenig, R. M. Hardesty, C. J. Senff, M. A. Krainak, J. B. Abshire, H. E. Bravo, S. P. Sandberg, "Preliminary measurements with an automated compact differential absorption lidar for the profiling of water vapor," Appl. Opt. **43,** 3110–3121 (2004).
18. A. R. Nehrir, K. S. Repasky and J. L. Carlsten, "Micropulse water vapor differential absorption lidar: Transmitter design and performance," Opt. Express **22,** 25137–25151 (2012).
19. K. Numata, J. R. Chen, S. T. Wu, J. B. Abshire and M. A. Krainak, "Frequency stabilization of distributed-feedback laser diodes at 1572 nm for lidar measurements of atmospheric carbon dioxide," Appl. Opt. **50,** 1047–1056 (2011).
20. M. Hamilton, R. Atkinson, A. Dinovitser, E. Peters and R. A. Vincent, "Towards low-cost water-vapour differential absorption lidar," Proc. SPIE **7153**, 71530C (2008).
21. H. R. Khalesifard, A. Fix, G. Ehret, M. Schiller, and V. Wulfmeyer, "Fast-switching system for injection seeding of a high-power Ti:sapphire laser," Rev. Sci. Instrum. **80**, 073110 (2009).
22. F. Spath, S. Metzendorf, A. Behrendt, H.-D. Wizemann, G. Wagner and V. Wulfmeyer, "Online/off-line injection seeding system with high frequency-stability and low crosstalk for water vapor DIAL," Opt. Commun. **309**, 37–43 (2013).
23. A. Dinovitser, M. Hamilton and R. Vincent, "Stabilized master laser system for differential absorption lidar," Appl. Opt. **49,** 3274–3281 (2010).
24. D. R. Herriott and H. J. Schulte, "Folded optical delay lines," Appl. Opt. **4,** 883–891 (1965).
25. D. S. Bomse, A. C. Stanton and J. A. Silver, "Frequency modulation and wavelength modulation spectroscopies: comparison of experimental methods using a lead-salt diode laser," Appl. Opt. **31** 718–731 (1992).
26. R. W. P. Drever, J. L. Hall, F. V. Kowalski, J. Hough, G. M. Ford, A. J. Munley and H. Ward, "Laser phase and frequency stabilization using an optical resonator," Appl Phys B. **31** (2) 97–105 (1983).
27. J. M. Supplee, E. A. Whittaker and W. Lenth, "Theoretical description of frequency modulation and wavelength modulation spectroscopy," Appl. Opt. **33** 6294–6302 (1994).
28. J. A. Silver, "Frequency-modulation spectroscopy for trace species detection: theory and comparison among experimental methods," Appl. Opt. **6** 707–717 (1992)
29. A. Dinovitser *A Stabilized Master Laser System for Differential Absorption LIDAR,* University of Adelaide, Australia, PhD Thesis (2012).
30. P. Zhimin, D. Yanjun, C. Lu and Y. Qiansuo, "Odd harmonics with wavelength modulation spectroscopy for recovering gas absorbance shape," Opt. Express **20** 11976–11985 (2012)
31. L. G. Wang, D. A. Tate, H. Riris and T. F. Gallagher, "High-sensitivity frequency-modulation spectroscopy with

#243917 Received 30 Jun 2015; accepted 13 Aug 2015; published 21 Aug 2015

a GaAlAs diode laser," J. Opt. Soc. Am. B. **6** 871–876 (1989).
32. A. L. Chakraborty, K. Ruxton, W. Johnstone, M. Lengden and K. Duffin, "Elimination of residual amplitude modulation in tunable diode laser wavelength modulation spectroscopy using an optical fiber delay line," Opt. Express **17** 9602–9607 (2009).
33. V. Pevtschin and S. Ezekiel, "Investigation of absolute stability of water-vapor-stabilized semiconductor laser," Opt. Lett. **3,** 172–174 (1987).
34. S. Schilt, L. Thevenaz and P. Robert, "Wavelength modulation spectroscopy: Combined frequency and intensity laser modulation," Appl. Opt. **33,** 6728–6738 (2003).
35. W. J. Schwenger and J. M. Higbie, "High-speed acousto-optic shutter with no optical frequency shift," Rev. Sci. Instrum. **83**, 083110 (2012).
36. R. Matthey, S. Schilt, D. Werner, C. Affolderbach, L. Thevenaz and G. Mileti, "Diode laser frequency stabilisation for water-vapour differential absorption sensing," Appl Phys B. **85,** 477–485 (2006).
37. S. Schilt, R. Matthey, D. Kauffmann-Werner, C. Affolderbach, G. Mileti and L. Thevenaz, "Laser offset-frequency locking up to 20 GHz using a low-frequency electrical filter technique," Appl. Opt. **47,** 4336–4344 (2008).
38. L. Greenspan, "Humidity fixed points of binary saturated aqueous solutions," Journal of Research of the National Bureau of Standards. A, Physics and Chemistry **81A,** 89–96 (1977).
39. OIML, "The scale of relative humidity of air certified against saturated salt solutions," Organisation Internationale de Métrologie Légale. **OIML R 121,** 1 (1996).
40. A. Wexler, "Vapor pressure formulation for water in range 0 to 100°C. A revision," J. Res. Natl. Bur. Stand. **80A,** 775–785 (1977).
41. A. L. Buck, "New equations for computing vapor pressure and enhancement factor," Journal of Applied Meteorology **20,** 1527–1532 (1981).
42. WMO, " Guide to meteorological instruments and methods of observation," World Meteorological Organization **8,** 14–25 (2008).
43. V. Wulfmeyer and C. Walther, "Future performance of ground-based and airborne water-vapor differential absorption lidar. I. Overview and theory," Appl. Opt. **40,** 5304–5320 (2001).
44. M. A. Krainak, A. W. Yu, G. Yang, S. X. Li and X. Sun, "Photon-counting detectors for space-based laser receivers," Proc. SPIE Quantum Sensing and Nanophotonic Devices VII, **7608** 760827 (2010).

1. Introduction

Differential Absorption Lidar (DIAL) is a powerful technique for both range resolved as well as integrated column measurement of an absorbing atmospheric trace gas [1]. This is an important remote sensing technique because of its potential to fill gaps in our understanding of atmosphere, biosphere and climate from ground based, airborne, and space based platforms [2]. Furthermore, it is a technique that offers significant versatility for its capability of range-resolved measurement of virtually any constituent in the atmosphere including aerosols, water vapor, methane and carbon dioxide. A large part of the renewed interest in DIAL stems from its capability to understand climate feedback mechanisms associated with rising temperatures in the atmosphere and bodies of water in the northern latitudes, which can potentially destabilize vast permafrost methane hydrate reservoirs [3].

DIAL is a laser radar technique that provides a range resolved measurement of a particular gas species in the atmosphere. In its simplest implementation, two laser wavelengths are transmitted sequentially, and the return pulse signals are acquired and accumulated into separate data channels. Each molecular species contains tens of thousands of individual spectral resonances due to multiple combinations of unique rotational and vibrational modes. Note that DIAL utilizes only one of these resonances, the precise wavelength of which is almost always exclusive of any other molecular species. The differential signal is obtained by tuning one on-line wavelength to the center of a molecular resonance. Another off-line wavelength is tuned away from the same resonance. At an optical wavelength of around 820 nm, an optical offset of around 15 GHz, or $\sim$30 pm, results in off-line attenuation of less than $\sim$3% of the on-line attenuation for most molecular resonances at standard temperature and pressure (STP), $T = 296$ K, $P = 101$ kPa.

With a 2-wavelength DIAL system, the number density of the absorbing species $n_a(r)$ can be

#243917 Received 30 Jun 2015; accepted 13 Aug 2015; published 21 Aug 2015

calculated from the two channel data using the Schotland approximation [4]. This uses effective on-line absorption cross-section σ_{on}, the off-line absorption cross-section σ_{off}, as well as the online N_{on} and off-line N_{off} photocounts from range r,

$$n_a(r) = \frac{1}{2\Delta r(\sigma_{\text{on}} - \sigma_{\text{off}})} \ln\left(\frac{N_{\text{on}}(r_1)N_{\text{off}}(r_2)}{N_{\text{on}}(r_2)N_{\text{off}}(r_1)}\right). \quad (1)$$

An interesting property of Eq.1, is that most of the terms present in a lidar equation, including transmitter power and receiver efficiency, are canceled out. Overlap function is also cancelled out where it is the same for all transmitted wavelengths. This has lead to the claim that DIAL is 'self-calibrating' [5]. However, it is sometimes overlooked that the effective on-line absorption cross-section σ_{on} is a convolution of the laser spectrum with the molecular spectral feature, where the laser may be subject to phase, frequency and amplitude noise sources that can significantly broaden the laser line shape [6]. For example, in our system, a stable narrow laser line was contaminated with a broad spectrum dominated by amplified spontaneous emission (ASE) of a Semiconductor Optical Amplifier (SOA). When convolved with the molecular spectral line, the effective absorption was reduced by $\sim$11%, as illustrated in Fig. 1.

Furthermore, the spectral line parameters published in comprehensive databases like HITRAN [7] is acquired or modeled using various techniques and is intended for numerous different applications. Therefore, its accuracy and reliability might not be adequate for some applications. For example, Table 1 illustrates a $\sim$17% change in cross-section over recent releases for one very strong line. More accurate data is available across some specific narrow spectral ranges eg: [8], however, these generally do not include desirable DIAL wavelengths. Therefore, the effective absorption cross-section of a specific resonance line needs to be known for quantitative number density $n_a(r)$ measurements, and HITRAN is not necessarily a suitable reference for this data. For this reason, we developed a specific calibration technique based on *in-situ* measurements, and demonstrated its application to the DIAL system described in this paper.

Although 2-wavelength DIALs are the simplest type, there are some significant advantages to utilizing more wavelengths. A weak absorption line provides greater range, while a stronger line provides a larger differential signal, and therefore better accuracy at short range. One way to optimize DIAL range and accuracy at different gas concentrations, is to access absorption lines of different strengths. Alternatively, a single strong absorption line can be utilized, with multiple side-line wavelengths tuned slightly off-resonance for the desired optical depth, to provide the adjustable range and sensitivity [9]. Atmospheric pressure affects both the position, as well as the width of all molecular resonances. Figure 2 illustrates how slight off-resonance stabilized light can bypass much of the resonant attenuation at high altitude, while still be on-resonance at the lower altitudes, where atmospheric pressure shifts the molecular resonance towards the laser wavelength. The side-line technique can be used to harness the pressure-shift of a spectral line, to reduce absorption encountered at high altitudes, and is ideal for a nadir pointing or high altitude DIAL [10]. Space-based DIAL is a significant prospect, given the global coverage available to such an instrument, and developments in this field have long been considered for future generations of remote sensing instruments [11] [12]. This requires more than two stabilized lasers for online, side-line, and off-line wavelengths.

This paper presents an extension to our previously published novel two wavelength DIAL system, with one of the best DIAL wavelength fractional stability figures reported to date [13], for stabilizing three or more laser wavelengths with minimal additional components. We also present a calibration technique for water molecule cross-section, as a step towards quantitative DIAL measurement.

#243917 Received 30 Jun 2015; accepted 13 Aug 2015; published 21 Aug 2015

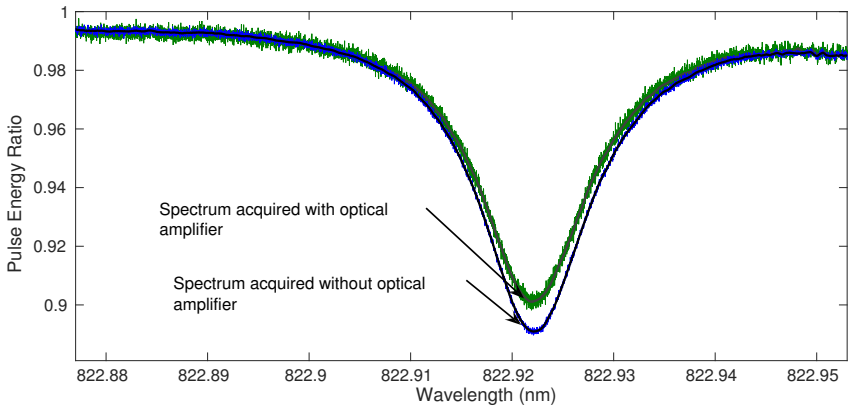

Fig. 1. Absorption spectra obtained using a wavelength scan with 1 μs optical pulses transmitted through our Herriott-like absorption cell. Transmitter and master lasers have different effective absorption cross-sections due to ASE from this optical amplifier in our transmitter. The absorption cross-section measurement described in the text, also calibrates the ASE, and is required for quantitative DIAL measurements. The effective absorption cross-section is calculated from a measurement of the attenuation through an open multi-path absorption cell of known length, and measured water molecule number density. The number density can be measured in various ways, we use a low-cost RH sensor calibrated against three saturated salt solutions as humidity references.

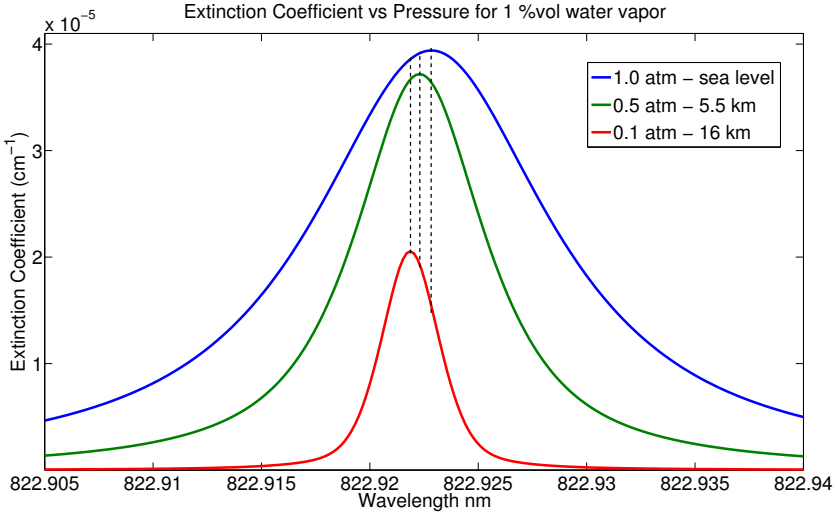

Fig. 2. Voigt model profiles of the 822.922 nm line at various altitudes including pressure shift, using HITRAN-08. As altitude increases and pressure decreases, pressure broadening and shift decrease. Lorentz broadening dominates at low altitudes, while Doppler broadening dominates at high altitudes. At 16 km, pressure is reduced by a factor of 10, while the peak absorption cross-section is reduced by a factor of only $\sim$2. Therefore, extinction can be significant despite the sparse atmosphere. Furthermore, for a small shift in wavelength (dotted vertical lines), the reduction in absorption cross-section is much greater at 16 km (red) than at sea level, STP (blue).

#243917 Received 30 Jun 2015; accepted 13 Aug 2015; published 21 Aug 2015

Table 1. Spectroscopic parameters of the 822.922 nm water line in recent HITRAN and ESA [14] database releases, illustrating the need for independent line-specific calibration for quantitative measurement

822.922 (nm)	Wavenumber $\nu(\mathrm{cm}^{-1})$	Intensity S_T $\times 10^{-23}(\mathrm{cm})$	Halfwidth $\gamma_a(\mathrm{cm}^{-1})$	Halfwidth $\gamma_s(\mathrm{cm}^{-1})$	Cross-section σ_p $\times 10^{-22}(\mathrm{cm}^2)$
HITRAN-06	12151.8198	3.848	0.0933	0.429	1.24
HITRAN-09	12151.8236	4.470	0.0915	0.432	1.47
HITRAN-12	12151.8223	4.470	0.0925	0.426	1.46
ESA-WV-14	12151.8235	4.660	0.0936	0.481	1.50

HITRAN spectroscopic parameter uncertainty is specified by I_{err} in the database, however, this does not define its actual accuracy bounds. This line has the lowest uncertainty value for I_{err}, however, recent database releases disagree with each other by up to 17% in terms of absorption cross-section. The vacuum wavenumber ν, intensity S_T and half-widths γ_a and γ_s come from the respective database releases, while the peak Voigt cross-section σ_p is calculated from the respective parameters using the Whiting-Olivero [15] [16] method, with Doppler, air- and self-broadening at STP and a volume mixing ratio of 0.9%.

2. This DIAL system

This design employs separate continuously stabilized diode lasers for each wavelength, with output pulses formed by optically switching the light from each diode laser at a time, to the input port of a tapered Semiconductor Optical Amplifier (SOA). The SOA is simultaneously energized to amplify the laser light, as illustrated in Fig. 3, with a low duty cycle of ∼1:1000. The on-line wavelength is stabilized to the targeted resonance line using an absorption cell, while the side-line and off-line wavelengths are beat-frequency stabilized using passive microwave bandpass filters. The central timing block drives all elements of the system including optical switching, data acquisition, and wavelength control system. This synchronous design, together with the use of passive references and ratiometric measurement, implemented with fiber optics, provides for a robust and accurate stabilization system at a minimal cost. The following sections describe the system in more detail.

2.1. On-line wavelength stabilization techniques

Wavelength stabilization can be achieved using calibrated references such as etalons [17] or wavemeters [18], or using absolute references such as gas absorption cells [19] [20]. Most recent work in this field focuses on using wavemeters for optical frequency stabilization [21] [22] that are easier to realize, however, they can also be subject to long-term drift unless calibrated with a gas reference cell. Alternatively, a gas cell reference can be employed for direct wavelength stabilization [23]. These are simpler and offer the best accuracy and long-term stability, although they are more difficult to utilize in practice. However, these systems may be better suited for applications that require robust and long term reliability with minimum power consumption, desirable for space-based application. We utilize a modified Herriott multi-pass absorption cell [24], open to the ambient humid air, as an absolute optical frequency reference for a water vapor resonance line.

Where a gas reference is directly used for laser stabilization, there are several techniques for stabilizing the wavelength to a single spectral line. These include modulating the injection current of the diode laser [25], or by applying external phase modulation outside the laser cavity [26] [27] to produce sidebands within the absorption feature. Injection current wavelength

#243917 Received 30 Jun 2015; accepted 13 Aug 2015; published 21 Aug 2015

modulation is the simplest modulation technique, but it is not always used for spectral measurements because the simultaneous power modulation results in an asymmetry of the signal line shape about the center absorption wavelength [28]. This Intensity Modulation (IM) effect is undesirable because it results in an offset in the measured position of the resonance, resulting in off-resonance stabilization, particularly with a broad absorption feature. For example, our system suffers a 590 MHz offset from resonance if stabilized in this way [29]. There are several common techniques for suppressing this effect including FM spectroscopy where a low modulation index m and a high modulation frequency ω_m are exploited to reduce this offset. A higher-harmonic demodulation [30] can also reduce this offset error. However, these techniques result in a significant trade-off in the available signal, that makes them unsuitable for accurate stabilization to weaker lines, or requires a longer path absorption cell [25]. Furthermore, the electro-optic phase modulators used in these systems add cost and complexity, and do not always completely eliminate IM due to practical amplitude and polarization modulation [19]. Other IM suppression techniques including two-tone modulation [31], and subtractive suppression using optical phase cancellation [32], also have major disadvantages for a robust, low cost DIAL. These considerations motivate the development of a DIAL optimized system, as described in this paper.

The on-line laser needs to be accurately stabilized to the molecular resonance wavelength, with an accuracy that depends on a number of variables, including the desired level of uncertainty of the retrieved profile and the actual width and shape of the absorption line at the maximum targeted altitude. Modeling has previously shown that a 1% accuracy of number density up to an altitude of 4 km, requires an absolute on-line optical frequency accuracy better than 50 MHz [29], an order of magnitude better than the stabilization accuracy with direct injection current modulation. Our system achieves an absolute stabilization accuracy better than ±60 MHz (measurement limited by the HighFinesse-Ångstrom-WS7 wavemeter), without any offset nulling or temperature compensation. This is achieved by solving the IM problem in a different way. With this design, there is no need to optically suppress IM, because its affect is directly rejected from the control system. Unlike the linear subtractive technique [33], this ratiometric technique employs analog division rather than subtraction of two signals, which requires no gain adjustments and suppresses the IM signal over a wider dynamic signal range.

Whereas the linear subtraction is merely used to reduce IM for higher order demodulation [34], the ratiometric technique eliminates the IM from the measured signal directly, enabling fundamental ($1f$) detection and a large modulation depth. Furthermore, this design is largely insensitive to offset drift in the electronics. However, it should be noted that the absolute accuracy was measured without the optical switching. Our AOMs shift the optical frequency by 80 MHz, which reduces the absorption cross-section by approximately 2%. This may be calibrated out, or it may be utilized for compensating atmospheric pressure shift of the spectral line. Alternatively, the optical switching can be carried out in different ways, without introducing any optical frequency shift [35].

The on-line detection and stabilization technique illustrated inside the control system in Fig. 3, consists of a pellicle or wedge beamsplitter, the multi-pass absorption cell, a pair of low-speed photodiodes and an analog divider. One photodiode measures the power entering the absorption cell without introducing any fringes, and the other photodiode measures optical power exiting the absorption cell. By instantaneously dividing the measured optical power before and after passing through the absorption cell, the output of the divider rejects any optical power modulation before the absorption reference cell. This rejects the IM due to the laser diode, as well as any IM due to the fiber optic and other optical components before the absorption cell.

However, the length of the absorption cell introduces a time delay (τ) between the two photodiode measurements and result in an offset error. Using a model of our laser diode and stabi-

#243917 Received 30 Jun 2015; accepted 13 Aug 2015; published 21 Aug 2015

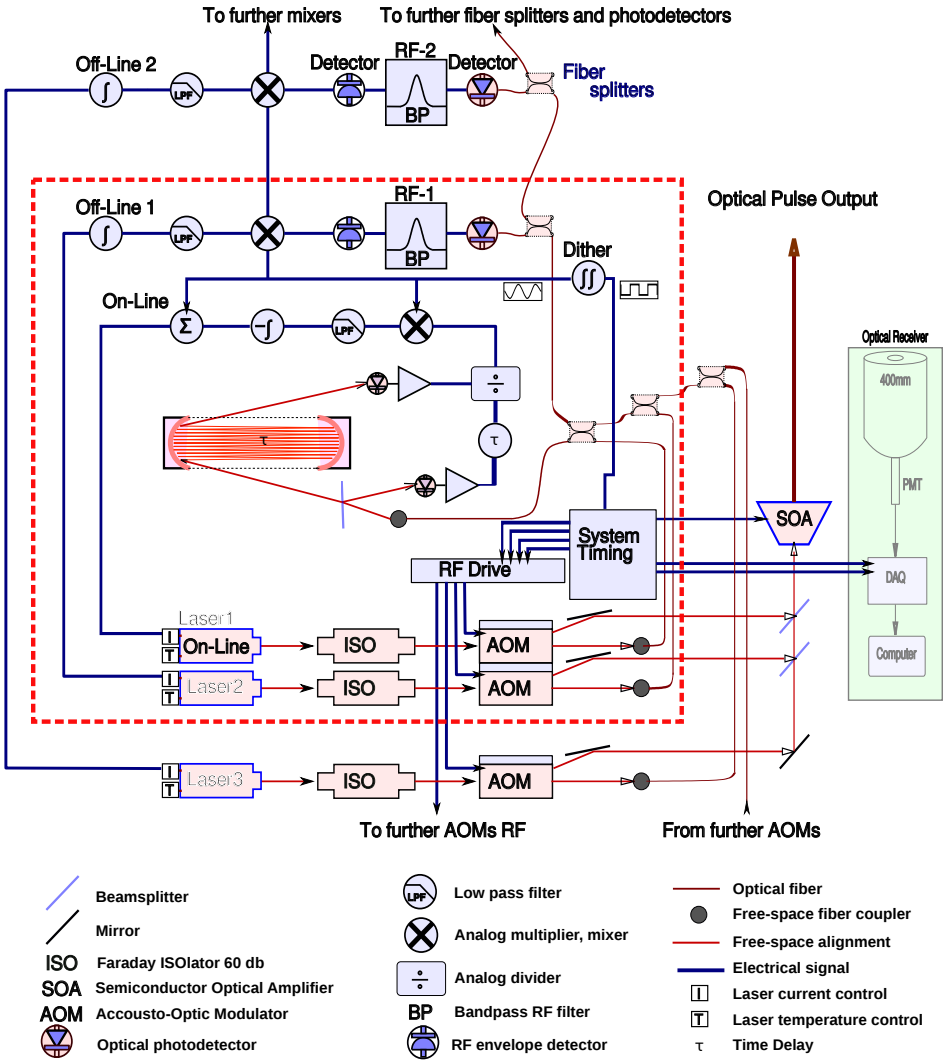

Fig. 3. DIAL control system showing the on-line laser stabilization system, two off-line stabilization systems, and arrows indicating additional layers to scale the system to any number of additional off-line or side-line wavelengths. The system enclosed by the red dashed square is equivalent to the original 2-wavelength design [23], with the on-line laser at the 822.922 nm water resonance, and one off-line stabilized by a 16 GHz optical beat frequency, equivalent to a ∼30 pm offset. The wavelength stabilization loops use a lock-in amplifier consisting of an analog mixer (AD633) and low-pass filter. 16 GHz beat frequency is measured by a bandpass filter RF-1 to stabilize the second laser to the desired optical frequency offset. Similarly, a third laser is stabilized with a bandpass filter RF-2. The transmitted pulse is formed as the timing system energizes an Acousto-Optic Modulator (AOM, Crystal Technology 3080-120) to briefly switch the light out of each laser control system, while simultaneously energizing a tapered Semiconductor Optical Amplifier (SOA, Sacher Lasertechnik TEC-400-830-500) to form the 1 μs output pulse with a 5%–95% rise and fall transition time of 8 ns. Atmospheric observations described here are performed using two wavelengths, with each wavelength firing at 1.5 kHz for a transmitted pulse repetition rate of 3 kHz.

#243917
Received 30 Jun 2015; accepted 13 Aug 2015; published 21 Aug 2015

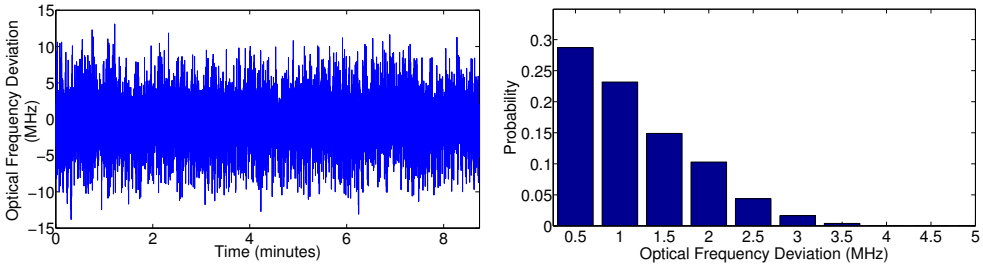

Fig. 4. This figure and histogram illustrate the optical frequency deviation of the on-line master laser from the water vapor resonance line of less than 2 MHz RMS, and the performance of the on-line wavelength stabilization system built with low cost general purpose components, eg: TL074 operational amplifiers. The $1f$ demodulation together with a deep 500 MHz wavelength modulation, results in a strong error signal and the excellent relative stability. This measurement is made with a sampling rate of 100 Hz for 10 minutes, over a bandwidth of 2 mHz to 50 Hz. This measurement is performed from the noise in the control loop, and does not capture fast optical frequency fluctuations and broadening of the optical spectrum, however, these are measured by the effective absorption cross-section, as discussed in Section 3.

lization system with 1.5 kHz dither, a 33-m absorption cell and 0.5% water vapor at STP, we expect an optical frequency offset close to 10 MHz [29], which is not significant for DIAL. However, by implementing the divider in firmware, the time delay due to the multi-pass cell is subtracted, and the residual 10 MHz error is eliminated, which facilitates the use of longer absorption cells and higher dither frequencies.

2.2. *Off-line or side-line wavelength stabilization techniques*

There are several published beatnote off-line laser wavelength stabilization systems including [36] and [37], that employ active microwave electronics with a local microwave oscillator for downconversion, followed by low-pass filter demodulation. We use a passive bandpass filter design for each off-line wavelength, as illustrated in Fig. 4, minimizing system cost and complexity.

In this implementation, fiber splitters combine all of the laser light sources, producing a beatnote from the on-line, and each off-line wavelength. The beatnotes are converted to a microwave signal that is measured with each bandpass filter. The off-line wavelengths are continuously stabilized with an error signal that is generated in a similar way to the on-line system. Since the dither is already present in the beat frequency signal due to the on-line control system, no further off-line wavelength modulation is required to produce every respective error signal in each of the off-line stabilization channels. In other words, only the on-line control system requires modulation to generate the error signal, which is also present in the beatnote, without any additional off-line wavelength modulation. Furthermore, since there is no modulation of the off-line wavelengths, there is no dither present in any of the beatnotes that are generated due to the mixing of the different off-line wavelengths, preventing any crosstalk between the off-line channels. Therefore, each of the off-line wavelengths is stabilized with a fixed offset from the on-line wavelength, set by a passive microwave bandpass filter, while the on-line wavelength is accurately stabilized to the center of a molecular spectral feature.

#243917 Received 30 Jun 2015; accepted 13 Aug 2015; published 21 Aug 2015

2.3. Timing and synchronization

Another unique novel element of our design is the way in which the dither modulation signal is generated, and how the timing system is used to minimize optical switching perturbation of the stabilization systems.

Figure 3 illustrates the synchronous system design where a sinusoidal modulation dither frequency is generated from the system timing clock by double integration, resulting in a 180° phase shift that accurately places each zero-crossing of the modulation signal at a timing transition. In this way, the wavelength modulation is synchronous with the optical switching and the optical pulses are formed at the same phase angle of the dither signal during each cycle. Furthermore, synchronizing optical switching with the zero-crossing of the wavelength modulation has two more benefits. Firstly, any offsets due to the the 500 MHz optical modulation, are eliminated from the optical pulses that are transmitted to the atmosphere. Secondly, as the stabilization error signal is the filtered instantaneous product of the modulation and the optical signals, optical switching transient at this point in time has a minimal effect the output of the multiplier as it occurs at the same instant when the modulation is near zero. Therefore, optical switching has minimal effect on the wavelength control systems, and does not significantly effect the accuracy of the wavelength stabilization systems. However, the wavelength sweep rate is at a maximum at this point in time, which produces a $\sim$1 MHz optical frequency chirp during the 1 μs pulse. However, this is not significant for DIAL.

3. Calibration

The calibration of effective absorption cross-section required for Eq.1, is carried out by measuring the on-line extinction (or transmission) through a known path length, as well as the measurement of molecular number density of water in the laser light path. The transmission measurement utilizes the same known path-length of the absorption cell, as well as the pulsed power output that is otherwise sent to the atmosphere. The measurement of the local water molecule number density is carried out using a calibrated sensor. This section illustrates the application of common meteorological equations for water vapor, for the calculation of effective absorption cross-section, and a calibration of the observation.

3.1. Transmission measurement

Measurement of the effective absorption cross-section of a water molecule is carried out by re-arranging the atmospheric observation system illustrated in Fig. 3, to the calibration system illustrated in Fig. 5.

The master laser diode control loop is opened and the laser wavelength is scanned across the absorption by changing its temperature, over a period of several seconds. Each of the 1 μs pulses are digitized into 256 samples with 12-bit resolution at 100 Ms^{-1} using a Gage CS14105 data acquisition card. A ratiometric technique is then implemented in software to suppress the effects of amplitude modulation due to the laser, SOA and etalon effects of other optical components, in a similar way to the analog ratiometric technique described in Section 2. With data acquired from both sides of the absorption cell, the significant 110 ns propagation delay of the absorption cell is compensated by shifting the un-delayed channels by eleven samples. The spectrum is obtained by concatenating 10^4 pulses, and Savitzky-Golay filtering is applied to the spectrum to facilitate the transmission measurement of the absorption line, relative to transmission on the wings. The result is illustrated in the top curve in Fig. 1.

From this result, the relative on-line transmission is measured to be $\mathbb{T} = 0.885$. This is related to the number density $\mathbb{N}$ and the molecular absorption cross-section σ,

#243917 Received 30 Jun 2015; accepted 13 Aug 2015; published 21 Aug 2015

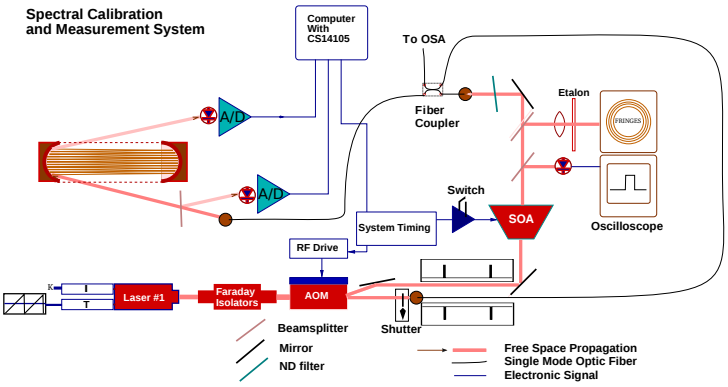

Fig. 5. System layout used to acquire data in Figure 1 as well as for the calibration. A thin etalon produces fringes when the light is coherent, which is used to align the Semiconductor Optical Amplifier (SOA) by maximizing fringe contrast. For the calibration, pulses from the SOA are acquired from both input and output of the vapor cell, as the laser temperature and wavelength are scanned across the absorption line. Signal processing in software is then used to perform the delay time compensation, as well as division for the ratiometric measurement of the absorption signal. From this measurement, the relative ratio of on-line and off-line attenuation is measured to calculate the extinction, that is used to calculate the effective absorption cross-section.

$$\mathbb{T} = \frac{I}{I_0} = \exp(-\mathbb{N}\sigma L), \tag{2}$$

where L is 33 m.

3.2. *Number density measurement*

A Relative Humidity (RH) sensor (Honeywell HIH4000) was calibrated against three fixed point humidity references [38] in accordance with Organisation Internationale de Métrologie Légale (OIML) guidance [39]. This measurement, together with temperature measured with a precision mercury thermometer, was used to calculate the molecular number density in Table 2, which was used to calculate the effective absorption cross-section of the laser.

The partial pressure of water vapor is given by

$$e' = U \cdot e_s/100 \tag{3}$$

where the relative Humidity (RH), U, and temperature T, is measured, and the saturation vapor pressure, e_s, given by [40] [41] [42],

$$e_s = \exp(-2991.2729T^{-2} - 6017.0128T^{-1} + 18.87643854 - 2.8354721 \times 10^{-2}T + 1.7838301 \times 10^{-5}T^2 - 8.4150417 \times 10^{-10}T^3 + 4.4412543 \times 10^{-13}T^4 + 2.858487\ln(T)) \tag{4}$$

where T is the measured temperature in Kelvin.

We now apply the ideal gas law to Eq. 3, to find the molar number, $n = e'/RT$, where $R = 8.3145\ \mathrm{JK^{-1}mol^{-1}}$,

and the absolute humidity, or number density per cubic centimeter, $\mathbb{N} = N \cdot n \times 10^{-6}$,where $N = 6.022 \times 10^{23}$.

#243917 Received 30 Jun 2015; accepted 13 Aug 2015; published 21 Aug 2015

To relate this to radiosonde data, the mass mixing ratio is calculated, $r = 621.98e'/(p-e')$, where p is the total pressure in kPa.

Table 2. Number density ($\mathbb{N}$) and mixing ratio (r) calculated from RH and temperature measured during the observation experiment. Note how temperature and RH change significantly while number density remains constant.

Time (approx)	Sensor V_{out}	T °C	RH %	$r\,\frac{\text{g}}{\text{kg}}$	$\mathbb{N}$ cm^{-3}
19.30	2.48	19.4	44.2	6.24	247×10^{15}
21.00	2.64	17.8	48.4	6.19	246×10^{15}
23.30	2.47	19.5	44.0	6.24	247×10^{15}

3.3. Calibration results

Using the measured transmission results $\mathbb{T}$ from Section 3.1, and the water molecule number density $\mathbb{N}$ from Sections 3.2, we thus have the measured effective absorption cross-section σ_{eff}

$$\sigma_{\text{eff}} = \frac{-1}{\mathbb{N}x}\ln(\mathbb{T}) = 1.49\times10^{-22}\ \text{cm}^2. \tag{5}$$

We can now compare the measured effective absorption cross-section σ_{eff}, with the calculated molecular absorption cross-section given in Table 1. Based on the results in Fig. 1, we can confidently say that the actual molecular absorption cross-section is at least 10% higher than the effective absorption cross-section calculated in Eq. 5. Therefore, the measured molecular absorption cross-section is at least 1.6×10^{-22} cm^2, which is $\sim$10% higher than the latest HITRAN or ESA model results. However, our result is in better agreement with the most recent databases, and this discrepancy is in line with the data variation in Table 1.

4. DIAL results

Atmospheric observations were performed by setting up the apparatus indoors, and directing the transmitter and receiver at a window to utilize an external mirror as illustrated in Fig. 6. on-line and off-line photon count data was acquired with the wavelength stabilization system arrangement as illustrated in Fig. 3.

Using the measured value for the effective absorption cross-section, as well as the raw data presented in Fig. 7, the number density and mixing ratios from the DIAL results in Section 4 are presented in Figure 8. These are compared with the radiosonde data in Table 4 with 150 m averaging. The radiosonde data is acquired by the Australian Bureau of Meteorology as part of their routine observation from Adelaide Airport, with the launch time coinciding with the start of our observation. However, this is a different location, closer to the coast, and predominantly open ground, whereas our location in Adelaide city is 8 km away with a lower prevailing humidity than the Airport, at ground level. Table 4 indicates this discrepancy, which decreases at higher altitudes.

However, there are some problems with this layout configuration. Firstly, this lidar is effectively blinded in the first 150 m by mirror scatter and speckle, and we are not able to obtain measurements in the first 150 m and directly compare the DIAL result with the humidity sensor.

Secondly, even though the same optical amplifier is used for both wavelengths, the output beam parameter is not completely independent of its input alignment. With the quasi-monostatic system in Fig. 6, the overlap below $\sim$400 m is incomplete, and different transverse

#243917 Received 30 Jun 2015; accepted 13 Aug 2015; published 21 Aug 2015

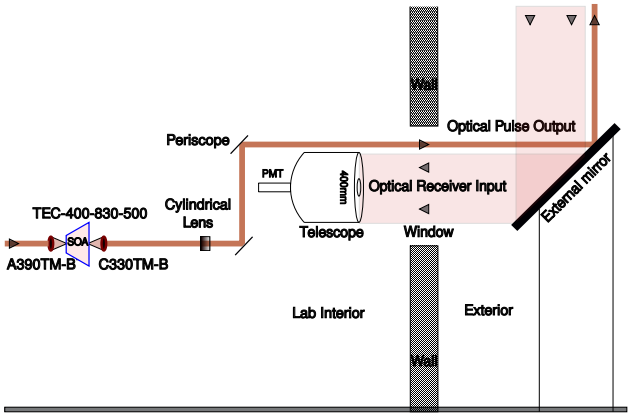

Fig. 6. Observation arrangement for atmospheric transmission. In order to direct the observation vertically through the atmosphere, the astigmatically corrected and collimated beam is directed by periscope to a large external mirror, mounted at 45° outside. Both the transmitted and scattered return light are reflected off this mirror.

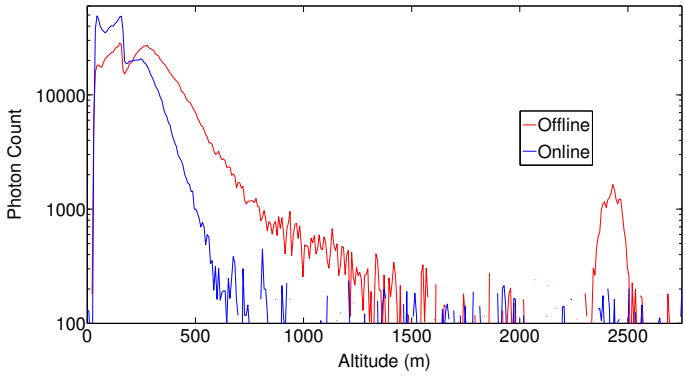

Fig. 7. Figure illustrating the integrated photon count vs range with one off-line wavelength offset by 16 GHz from on-line. The first 1 μs (150 m) of return data is invalidated by the scatter from the external mirror due to the arrangement illustrated in Fig. 6, with wavelength-specific difference likely due to speckle and chirp in the 1 μs pulse. Differential attenuation in the on-line (blue) and off-line (red) curves is visible up to 1 km, however, noise in the data precludes meaningful results past 700 m. Cloud backscatter at 2.4 km only appears in the off-line channel illustrating complete attenuation of the on-line signal at that range. A change in the shape of the off-line profile indicates the location of the boundary layer up to $\sim$1 km, characterized by its aerosol and moisture content. This low-power system relies on the boundary layer aerosols to acquire a return signal up to 1 km.

#243917 Received 30 Jun 2015; accepted 13 Aug 2015; published 21 Aug 2015

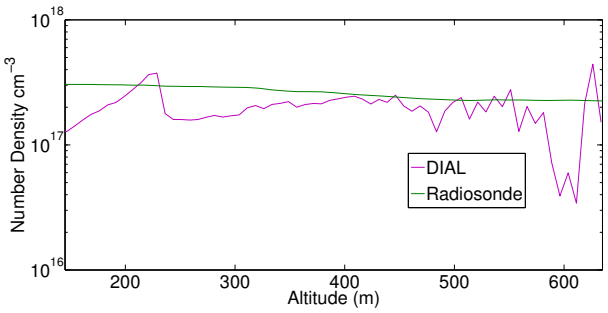

Fig. 8. Figure illustrating DIAL inversion of the data illustrated in Fig. 7, as well as the radiosonde data. Poisson statistics were used to slightly increase the available range. As the altitude increases, and so the intensity of the scattered pulse falls, ambient light and the dark count become a substantial fraction of the measured count, introducing a significant bias into the measurement. To correct for this, we measure the dark count during the period immediately before the pulse is transmitted. As this measurement is itself random, we construct an estimator for the unknown additional scattering count, rather than simply subtracting it from the measured values. Since photon counts are discrete, we use Poisson statistics, and thus *maximum-a-posteriori* estimation with an uninformative uniform prior on the scattering rate $\hat{\lambda}_s$ yields $\hat{\lambda}_s = \max\{0, \hat{\lambda} - \hat{\lambda}_d\}$. It should be noted, however, that this process itself yields a slightly biased estimator, and therefore if further filtering is to be performed, then it may be desirable to use the unbiased estimator $\hat{\lambda} - \hat{\lambda}_d$.

mode characteristics in the transmitter at the different wavelengths, may result in some DIAL errors. This may be responsible for the discrepancy with radiosonde data at lower altitudes, both in Fig. 7 and Table 4. A true monostatic arrangement will eliminate this source of error.

Also, the results in Fig. 7 illustrate a high water number density and line strength resulting in excessive on-line attenuation from $\gtrsim$700 m. In a DIAL application, a strong line produces a larger differential signal from each range cell, but suffers increased attenuation which limits the measurement range. Therefore, a suitable line strength is a trade-off between range and precision. The resolved range cell extinction during this observation was around 0.4, whereas an extinction between 0.03 and 0.1 is optimal [43].

However, the main reason for the short range, is the low pulse energy of our transmitter (0.3 μW), as well as the low 5% quantum efficiency of our Photomultiplier Tube (PMT) detector-filter combination (Hamamatsu R7400U-20) at this wavelength. A cooled Silicon Avalanche Photodiode (APD) will provide and order of magnitude increase in sensitivity [44], while an additional laser amplifier can provide another 2-orders of optical gain for a vertical range to 5 km, useful data for operational meteorology.

5. Conclusion and future work

Differential Absorption Lidar is the perhaps most promising candidate for future active remote sensing of atmospheric composition from earth and from space. This paper presents two important elements towards a reliable, quantitative measurement system. We present a novel multi-wavelength DIAL seed laser system design, and illustrate its operation by application as a micropulse transmitter to obtain short-range measurements. Measurement with a $\sim$300 nanojoule transmitter and PMT detector are obtained up to 700 m, by calibration of effective absorption cross-section of water vapor resonance at 822.922 nm.

This seed laser system is a critical element of future DIAL. However, to build an operational DIAL observatory, work is now required on a suitable laser amplifier with significantly

#243917 Received 30 Jun 2015; accepted 13 Aug 2015; published 21 Aug 2015

Table 3. Comparison with radiosonde data from Adelaide airport. The low latitude radiosonde results show a higher water content than DIAL, as well as the humidity measured in our lab at this time. Such differences may be partly due to radiosonde calibration, as well as the local conditions at the airport that include mostly open grass, while the University campus ground is mostly sealed. Another interesting observation, is that the discrepancy seems to decline with altitude, as expected with more homogeneous atmospheric composition due to reduced ground effects. This discrepancy at low altitude was observed systematically during other observations.

Range (m)	Radiosonde mixing ratio ($\frac{g}{kg}$)	% difference
0–150	7.6	n/a
150–300	7.4	32
300–450	6.7	28
450–600	5.9	11

increased transmitter power and pulse energy. A transmitter with 20 dB gain, with an APD detector, will increase this range to ∼5 km. This increased range, accuracy and reduced averaging time, will provide useful data for operational meteorology.

This prototype master laser is also now ready for the next stage of development, including a fully digital implementation. The multiple wavelength stabilization system described herein may be applied to other types of lasers, operating at different wavelengths, to target CO_2, Methane, and other trace gas species in the atmosphere.

The techniques described in this paper are a step towards reliable, low-cost DIAL observatories, to provide quantitative measurements of atmospheric trace gases.

Acknowledgments

Support for this project, as well as useful discussions and interactions with Murray Hamilton and Robert Vincent are gratefully acknowledged.

#243917 Received 30 Jun 2015; accepted 13 Aug 2015; published 21 Aug 2015